Petroleum and Coal

Article **Open Access**

HYDROCARBON POTENTIALITY OF BIDA BASIN FROM HIGH RESOLUTION AEROMAGNETIC DATA

*O. D. Ajama[1], O. S. Hammed[2], S. C. Falade[1], A. B. Arogundade[1], O. M. Olasui[1], F. A. Olayode[1], O. T. Olurin[3] and M. O. Awoyemi[1]**

[1] *Department of Physics and Engineering Physics, Obafemi Awolowo University, Ile-Ife, Nigeria*
[2] *Department of Physics, Federal University Oye, Oye-Ekiti, Nigeria*
[3] *Department of Physics, Federal University of Agriculture, Abeokuta, Nigeria*

Received September 19, 2017; Accepted November 30, 2017

Abstract

In this study, High Resolution Aeromagnetic Data (HRAD) was analyzed to estimate the average geothermal gradient, sedimentary thicknesses and to delineate intrusives within the Northern Bida Basin with a view to ascertaining the hydrocarbon potential of the basin. The Curie Point Depth (CPD) estimation method revealed an average CPD of 20 km and an average geothermal gradient of 29°C/km for the study area. Oil and Gas windows within the study area were estimated to fall within the depth range of 2.1 – 4.1 km and 4.1 – 7.8 km respectively. Spectral Analysis and Source Parameter Imaging (SPI) techniques revealed the morphology of the basin and sedimentary thicknesses of over 2.0 km within Kudu, Takuma, Gbaki, Charati, Motugi and Jasegi environments. 2D forward modeling further revealed the presence of intrusives, as possible channels for the flow of geothermal energy, within Kudu and Takuma, whose sedimentary thicknesses fall within the Oil window. This study concluded that the study area may contain more oil than gas and that Kudu and Takuma regions are more promising for hydrocarbon generation than other potential locations.

Keywords: Aeromagnetic method; Curie point depth; hydrocarbon; source rock; intrusives.

1. Introduction

Over the years, the aeromagnetic method has proven to be a wonderful reconnaissance tool in mapping major structures within the earth's crust. In recent times, it has been widely employed at a regional scale to map potential areas for hydrocarbon exploration [1].

For exploration purposes, the use of residual maps for the identification of intrusives, lava flows and igneous plugs have proved viable [2]. These subsurface structures have implications for hydrocarbon generation and accumulation. For instance, igneous intrusions serve as channels for the flow of geothermal energy needed for maturation of petroleum source rocks from organic matter [3]. When many, they produce a large amount of heat energy in potential source rocks thereby increasing the temperature to a state which could be above requirement; in this case, over-maturation of source rocks, which causes a reduction in the amount of hydrocarbon generated, could occur. Nevertheless, Rateau *et al*. [4] reported that permeability in sills as a result of formation of cooling joints, fractures and, in very shallow-level intrusions, by the occurrence of interconnected gas vesicles could serve as conduits for hydrocarbon migration.

The Bida Basin (Figure 1), just like the Niger Delta Basin, is one of the sedimentary basins in Nigeria. Preliminary studies by Obaje *et al*. [5] from geochemical analyses of source rock samples obtained from shallow wells (≤71 m) drilled at Kudu, revealed that the source rocks samples from well location "Kudu51" at a depth of 51 m had an Hydrogen Indices of 402 mgHC/gTOC which is above the minimum value of 300 mgHC/gTOC needed for oil generation but its thermal maturity Tmax (430°C) is below the minimum value (435°C) required for oil generation. This low Tmax value could be related to the level of maturation of source rocks within

the basin which depends on temperature, time of exposure to temperature and pressure from sedimentary overburden among others. In order to assess the regional-scale hydrocar-bon potentiality of the Bida Basin, there is need for geophysical investigation of important parameters for source rock maturation which include sedimentary thickness, geothermal gra-dient and the presence of intrusives within the basin.

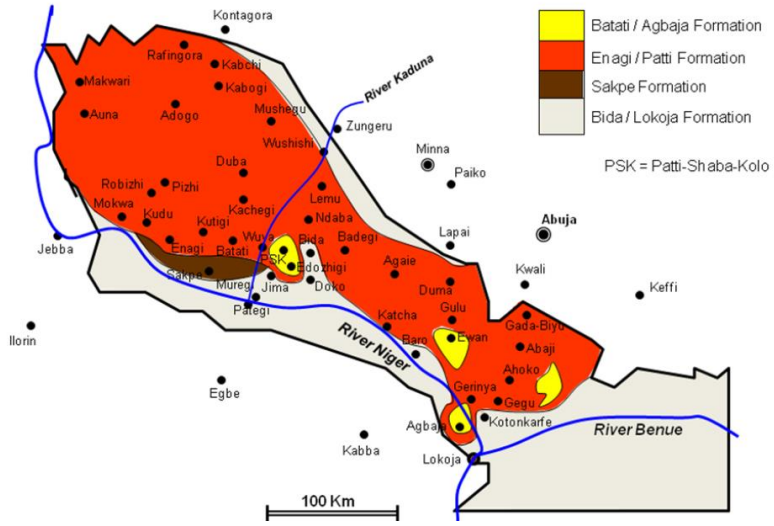

Figure 1. Surface Geology of the Bida Basin (Adapted from Obadje *et al*., 2013)

2. Sedimentation and stratigraphy

The basin's strata (Figures 1 and 2) are upper (late) Cretaceous in age and referred to as the Nupe Group. The group encompasses a two-fold Northern/Central Bida Basin and Southern Bida Basin. The focus of this research work is on the Northern/Central section of the basin. The Central Bida Basin is made up of four formations namely the Bida Sandstone, the Sakpe Ironstone, the Enagi Siltstone, and the Batati Ironstone.

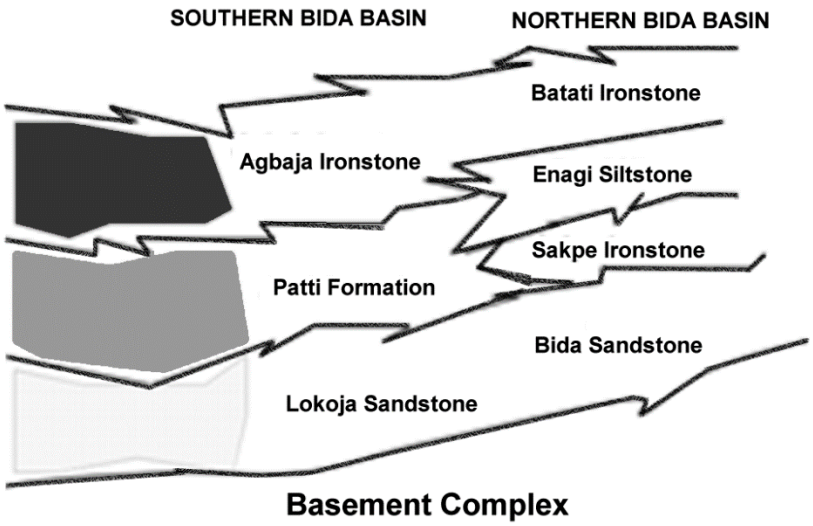

Figure 2. Stratigraphic Successions in the Bida Basin (*Adapted from Obadje et al., 2013*)

The Batati Formation, referred to as the Batati Ironstone Formation around Bida, is surrounded by the Enagi Siltstone at each surface exposure. The Batati Formation consists of argillaceous, oolitic and goethitic ironstones with ferruginous claystone and siltstone

intercalations and shaly beds occurring in minor proportions, some of which have yielded near-shore shallow marine to fresh water fauna [6].

The Enagi siltstone comprises mainly of siltstone which correlates with the Patti Formation in the Southern Bida Basin. Other supplementary lithologies include sandstone-siltstone admixture with some claystones [7]. The formation covers over 70% of the surface area of the basin. It contains a dark-grey, black shale unit, the Kudu Shale (Kudu Shale Member) envisaged to be the potential source rock for hydrocarbons in the northern section of the basin [5].

The Sakpe Ironstone comprises mainly oolitic and pisolitic ironstones with sandy claystones locally, at the base, followed by dominantly oolitic ironstone which exhibits rapid facies changes across the basin, at the top [5].

The Bida sandstone consists mainly of fine to coarse grained sandstones, conglomerates, siltstones and claystones. It is composed of two members, namely the Doko member and the Jima member. The Doko Member is the basal unit and consists mainly of very poorly sorted pebbly arkoses, sub-arkoses and quartzose sandstones [5]. The Jima member is majorly composed of cross-stratified quartzose sandstones, siltstones and claystones. It is the upper unit of the Bida Formation and exhibits similar features as the upper part of the Lokoja Sandstone. It has surface exposure at the northeastern and southwestern flanks of the basin.

3. Methodology

High Resolution Aeromagnetic Data (HRAD) of the Northern section of Bida Basin bounded by latitudes 8°30' to 10°00'N and longitudes 5°00' to 6°30' E was acquired from the Nigeria Geological Survey Agency (NGSA). The acquired data was gridded at 100 m spacing using the minimum curvature gridding method and knitted to produce the total magnetic intensity (TMI) map of the study area (Figure 3).

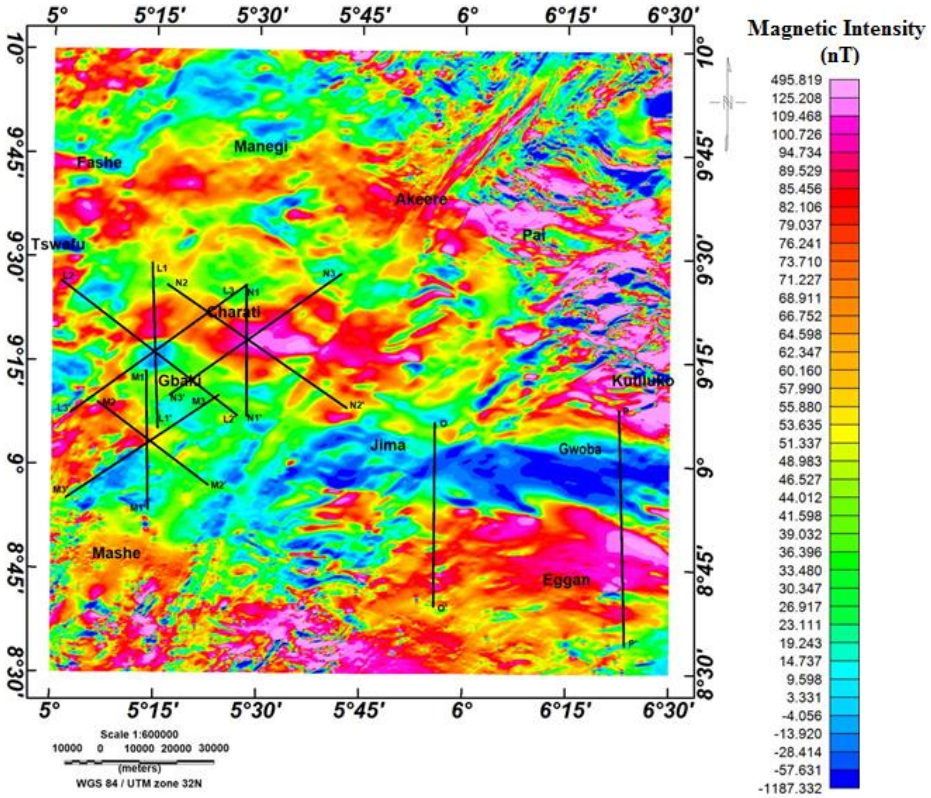

Figure 3. Total Magnetic Intensity map of the study area (to obtain the total value, add 33,200 nT to the values on the legend). Profile lines for modelling are shown

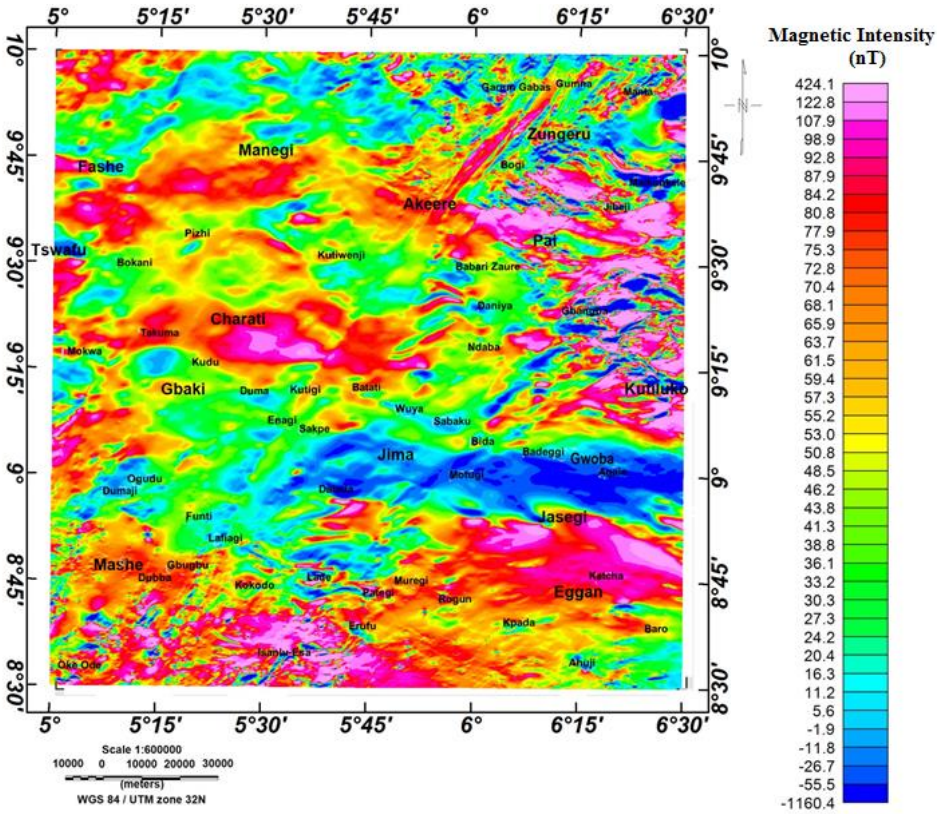

Figure 4. Reduced to the equator map of the study area

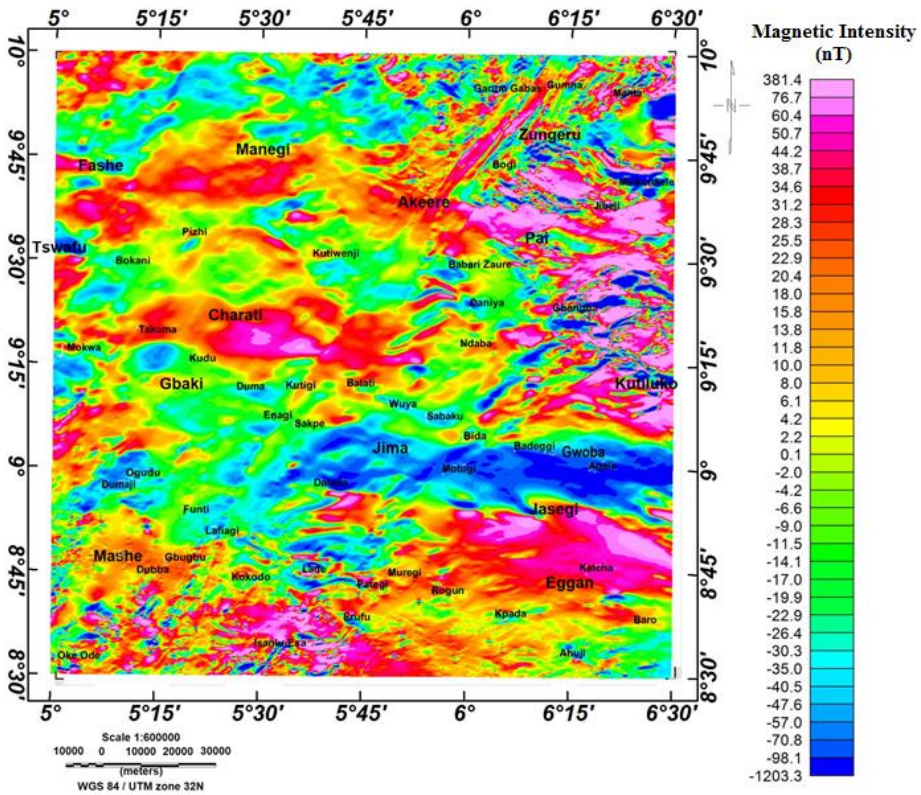

Figure 5. Residual magnetic intensity map of the study area

In equatorial regions where inclination is less than 15°, reduction-to-pole (RTP) of magnetic data causes the total field anomaly and any noise included within the measurements to experience high directionally selective amplification [8] in the north-south direction, thereby causing instability in the magnetic data [9]. A solution to this problem is to reduce the low-latitude magnetic data to the equator rather than to the pole. This centres the peaks of magnetic anomalies over their corresponding sources [10]. Thus, the TMI map of the study area was reduced to equator. The regional field corresponding to an upward continuation height of 32 km was removed from the Reduced to Equator (RTE) map (Figure 4) to suppress the long-wavelength components arising from regional and gross terrain features. The removal of the regional field from the RTE map generated the residual magnetic intensity (RMI) map of the study area (Figure 5). Thereafter, the average geothermal gradient of the study area was estimated from the Curie Point Depth determined from spectral analysis of the RTE map using centroid approach. Source Parameter Imaging (SPI) and Spec-tral Analysis (SA) techniques were both applied to the RMI map to estimate the sedimentary thicknesses of the study area. Based on the estimated sedimentary thicknesses and average geothermal gradient within the study area, potential areas for hydrocarbon generation were mapped out. Furthermore, 2D forward modelling of the subsurface was carried out along these areas to map intrusives and identify possible areas for hydrocarbon generation.

3.1. The Centroid method

The Curie Point Depth (CPD) is usually regarded as the theoretical surface with a temperature of about 580℃ where magnetized bodies become para-magnetic. Beneath this depth, the lithosphere virtually exhibits paramagnetic properties. Okubo *et al*. [11] developed a method to estimate the depth to magnetic bottom (Z_b) of magnetized bodies from the methods of [12-13].

Consider the case of a set of 2D bodies whose magnetization M(x,y) is completely random and uncorrelated, the power spectrum density of the magnetic anomalies could be written as [8,14]:

$$P(k) = A_1\, e^{-2|k|Z_t}\,(1 - e^{-|k|(Z_b - Z_t)})^2 \quad (1)$$

where A_1 is a constant, Z_b and Z_t are the depth to the bottom (Curie point depth) and top of the magnetic body respectively and k the wavenumber of the magnetic field.

The centroid depth (Z_c) (Figure 6a) of the deepest magnetic source is estimated from the slope of the longest wavelength part of the spectrum divided by the wavenumber using the equation [15]:

$$\ln\left(\frac{P(k)^{\frac{1}{2}}}{k}\right) = A - |k|Z_c \quad (2)$$

where $P(k)$ is the power density spectrum and A represents a constant.

The depth to the top of the magnetic source (Z_t) (Figure 6b) is similarly derived from the slope of high wave number portion of the power spectrum as following [15]:

$$\ln\left(P(k)^{\frac{1}{2}}\right) = B - |k|Z_t \quad (3)$$

where B is a constant.

The CPD (Z_b) is then obtained from

$$Z_b = 2Z_c - Z_t \quad (4)$$

The geothermal gradient (dT/dz) between the earth's surface and the CPD is given by the relation

$$\frac{dT}{dz} = \frac{580^{o}C}{Z_b} \quad (5)$$

The RTE map spanning about 165 km by 165 km was used as a single block to estimate the average CPD of the study area. The depth to the centroid (Z_c) and depth to the top (Z_t) of the magnetic sources were computed by linear fitting to the longest and second-longest wavelength segments of the frequency-scaled power spectrum (Equation 2) and unscaled power spectrum (Equation 3) respectively. Thereafter, the average curie point depth (Z_b) and the

average geothermal gradient for the study area were calculated using Equations 4 and 5 respectively.

3.2. Source Parameter Imaging (SPI) Technique

The SPI technique [16] is a wonderful tool for determining the thickness of sediment within a basin. It is useful in mapping potential regions for oil and gas prospecting. It utilizes the relationship between source depth and the local wavenumber (k) of the observed field, which can be calculated for any point within a grid of data. The SPI technique works for two models: a 2D sloping contact or a 2D dipping thin-sheet. For a magnetic field M, the local wavenuber, k, is given as

$$k = \frac{1}{|A|^2}\left(\frac{\partial^2 M}{\partial x \partial z}\frac{\partial M}{\partial x} - \frac{\partial^2 M}{\partial x^2}\frac{\partial M}{\partial z}\right) \quad (6)$$

where |A| is the analytic signal amplitude.

Nabighian [17] gave the expressions for the vertical and horizontal gradients of a sloping contact as

$$\frac{\partial M}{\partial z} = 2KFc\sin d \times \frac{x\cos(2I-d-90)-h\sin(2I-d-90)}{h^2+x^2} \quad (7)$$

$$\frac{\partial M}{\partial x} = 2KFc\sin d \times \frac{h\cos(2I-d-90)+x\sin(2I-d-90)}{h^2+x^2} \quad (8)$$

where K is the susceptibility contrast at the contact; F is the magnitude of the Earth's magnetic field; $c = 1 - \cos^2 i \sin^2\alpha$; α is the angle between the positive x-axis and magnetic north; I is the ambient-field inclination; $\tan I = \tan i/\cos\alpha$; d is the dip (measured from the positive x-axis); h_c is the depth to the top of the contact and all trigonometric arguments are in degrees.

Substituting equations (7) and (8) into the expression for the local wavenumber (6) gives

$$k^2 = \frac{h}{h^2+x^2} \quad (9)$$

where the coordinate system has been defined such that the origin of the profile line (x=0) is directly over the edge.

It is evident from equation (9) that maxima of the local wavenumber are independent of the magnetization direction. Thus, the peaks outline source edges, and at these locations $x = 0$. At $x = 0$, the "local depth" can be calculated using $h = \frac{1}{k}$ (10)

The local wavenumber, k, is used to determine the most appropriate model and a depth estimate independent of the assumed model.

3.3. Spectral Analysis (SA) method for depths to the basement

The RMI map of the study area was windowed to acquire forty-nine (49) overlapping windows with a size of about 42 km by 42 km. Each windowed grid was Fast Fourier transformed and the logs of the radially average spectrum was calculated and plotted against the corresponding wavenumbers. Two lines were fitted on the linear segments that correspond to the deep sources and shallow sources which are represented by the low wavenumber and high wavenumber segments of the spectrum respectively. The slope of each fitted segment was calculated and converted to depth H using the formula: $H = -\frac{s}{4\pi}$.

4. Results and discussion

4.1. Total Magnetic Intensity (TMI) Map

The TMI map shows short wavelength anomalies in the northeastern and southwestern edges of the study area which indicate that the study area is bounded by basement complex areas. Parts of these areas are covered by the Bida Sandstone Formation. They are more likely to be of shallow sedimentary cover and therefore less promising for hydrocarbon generation. The long, intermediate and short wavelength anomalies correspond to deep lying magnetic bodies, intrasedimentary intrusive bodies and shallow seated magnetic bodies/basement outcrops respectively. The observed variation in the surface magnetic anomaly could be attributed to susceptibility variations and topography of the magnetic sources within the study

area. Majority of the deep-seated basement rocks within the study area are overlain by the Enagi Siltstone Formation.

4.2. Reduced to Equator (RTE) and Residual Magnetic Intensity (RMI) Map

The RTE technique is used to center magnetic anomalies over their causative bodies in order to make interpretation simpler. Inspection of the RTE map shows that there is a reduction in the high positive magnetic intensity value (from 495 to 424 nT) when compared with the TMI map. This further reduces after the removal of the regional field to produce the Residual Magnetic Intensity Map (Figure 5). Due to the fact that the study area is in a low latitude region, locations with high amplitude and/or long wavelength anomalies (magenta colour) within the basin (e.g Charati and Jasegi) are most likely to be of lower susceptibility than their neighbouring environment. Based on the implication of long wavelength and high amplitude for depth and sedimentary thickness, the locations most likely have potential for hydrocarbon generation. The very low magnetic intensity value (blue colour) might be associated with intrusion onto the basement surface or within the sedimentary section of the study area.

4.3. The Curie Point Depth and geothermal gradient of the study area

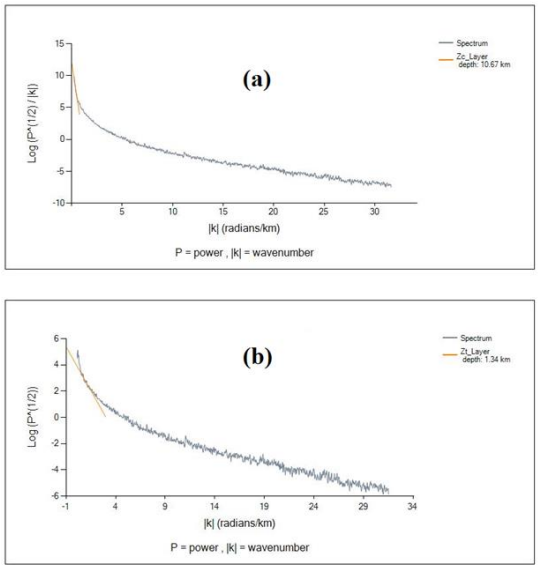

Figure 6. Plots of (a) Frequency-Scaled power spectrum (b) Power spectrum used for the determination of the Curie Point Depth of the study area

Figure 6 shows the frequency-scaled power spectrum and unscaled power spectrum from which Z_t and Z_c were estimated to be 1.34 km and 10.67 km respectively. The average Curie point depth (Z_b) and geothermal gradient for the study area were calculated from the obtained values of Z_t and Z_c to be 20 km and 29℃/km respectively. According to Selley[2] a significant crude oil generation occurs between 60℃ and 120℃ while a significant gas generation occurs between 120 ℃ and 225 ℃.The implication of this temperature range for depth, based on the average geothermal gradient ($29℃/km$) obtained for the study area, is that crude oil will occur at a depth window of 2.1 – 4.1 km, and gas at 4.1 – 7.8 km.

4.4.Sedimentary thicknesses

The SPI map of the study area is presented in Figure 7. It shows the variations of the sedimentary thickness within the basin. The magenta colour at the top of the SPI legend signify locations with shallow sedimentary thickness or near surface magnetic bodies while the deep blue colour at the lowest part of the legend signify locations with high sedimentary thickness or deep lying magnetic bodies. The shallow sedimentary thickness (< 0.2 km) at the north-eastern, southwestern and southern flanks of the study area suggests that these locations are basement complex areas. The deeper parts of the study area (> 2 km) extend diagonally from Fashe through Charati and Motugi to Jasegi. The Enagi formation makes up most of the surface sedimentary cover within the study area. It perhaps has the highest sedimentary thickness within the northern section of the Bida Basin. Based on the sedimentary thicknesses and average geothermal gradient obtained for the study area, enclosed regions 1 and 2 with depths over 2.0 km are potential regions for hydrocarbon generation. Profiles A - A', B - B' and C -

C ' were drawn within the enclosed regions for an enhanced view of their bedrock topography and depth. Figure 8 shows the depth variations along these profiles. Environments with hydrocarbon potential within these regions (indicated with blue rectangular symbols) include Gbaki, Kudu, Takuma, Charati, Motugi and Jasegi.

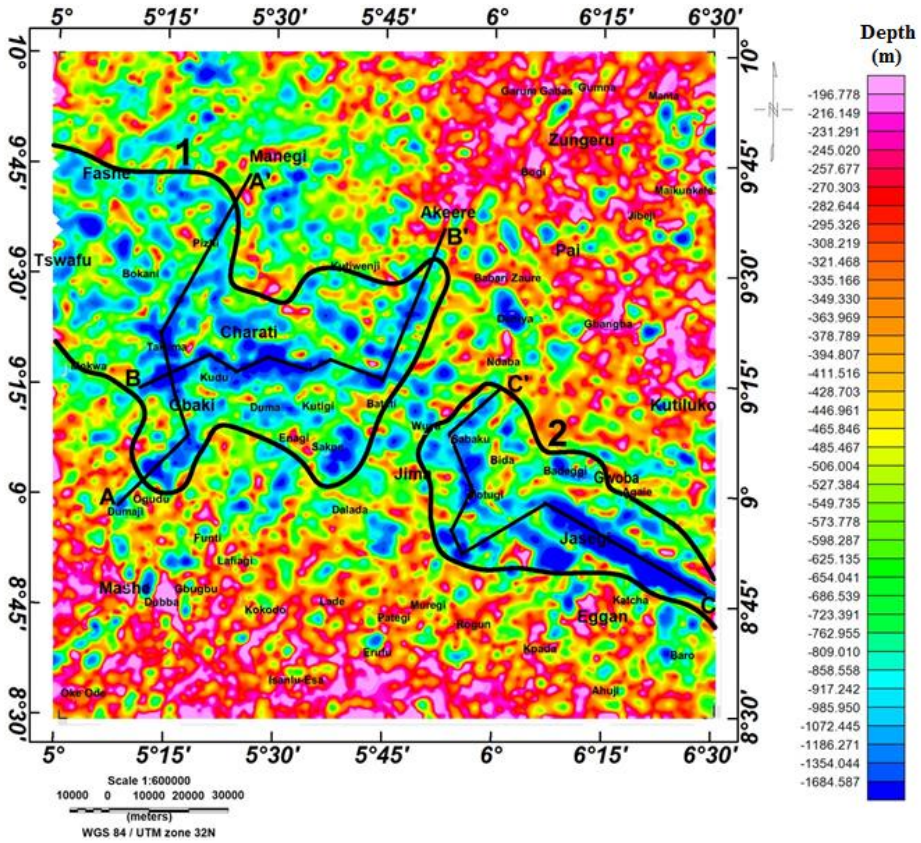

Figure 7. SPI Map of the Sedimentary Thickness within the Study Area. The closed regions 1 and 2 represent potential regions for hydrocarbon generation. Profiles A - A', B - B ' and C - C ' within the enclosed regions were drawn to highlight the sedimentatary thickness across the profile

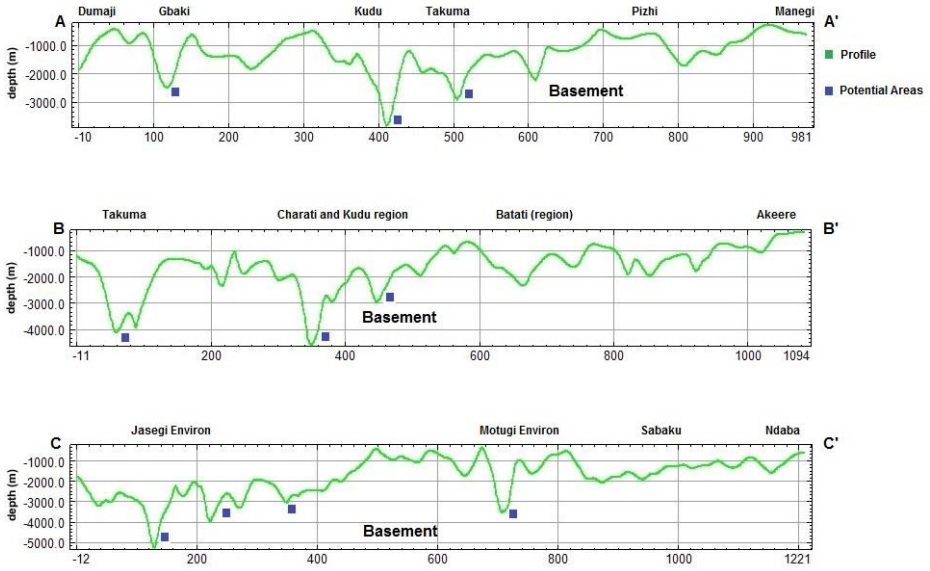

Figure 8. Sedimentary thickness and delineation of potential hydrocarbon areas along the profiles

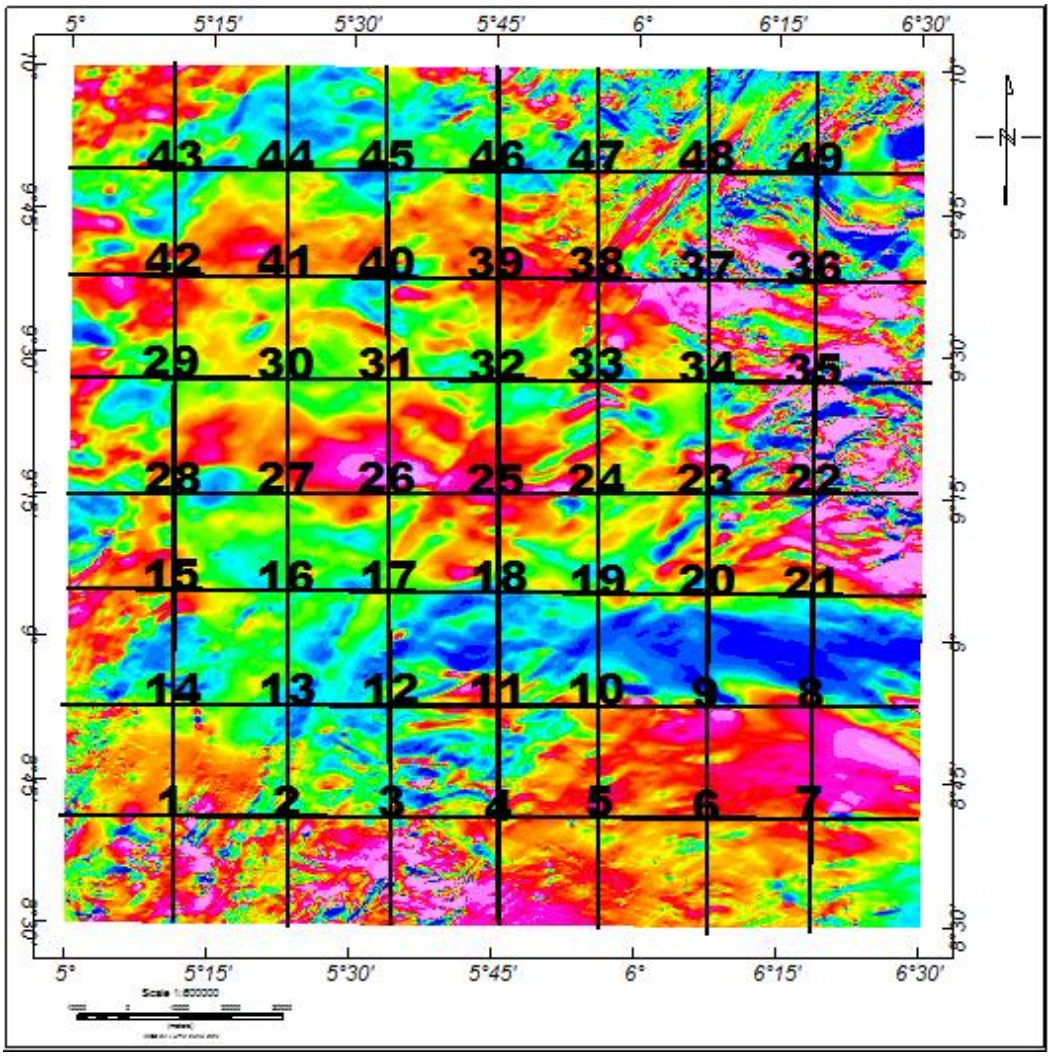

Figure 9. Windows for spectral depth of the study area extracted from the RMI map

Figure 9 shows the subdivision of the study area into forty-nine (49) overlapping blocks from which the average depth to magnetic source layers within each block was estimated through spectral analysis. Figure 10 shows a representative power spectrum for block 16. The results obtained for all blocks are presented in Table 1. Based on prior knowledge of the study area and in comparison with results obtained in previous studies on parts of the study area [18-19], the second layer of the power spectra represents the depth to basement (Figure 11) in the study area with a minimum value of 0.45 km and a maximum value of 3.41 km. The average thickness of the sedimentary formation that overlie the basement within the Bida Basin was estimated to be 1.13 km. The deepest region of the basin which is in the southeastern part (around Jasegi) has an average depth of 3.41 km to basement.

From the maps of SPI and SA, the areas with shallow depth to basement are noticeable in the northeastern, eastern, southwestern and southern edge of the study area. These areas are made up of the basement complex regions partly overlain by the Bida Sandstone. The sedimentary thickness increases from the southwestern and northeastern edges to the central portion of the study area. Gbaki, Kudu, Takuma, Charati and Jasegi environments appear to have the highest sedimentary thickness. Based on the average geothermal gradient of the study area ($29℃/km$) and the highest depth estimates from both SPI and SA methods, the study area may accommodate more oil than gas.

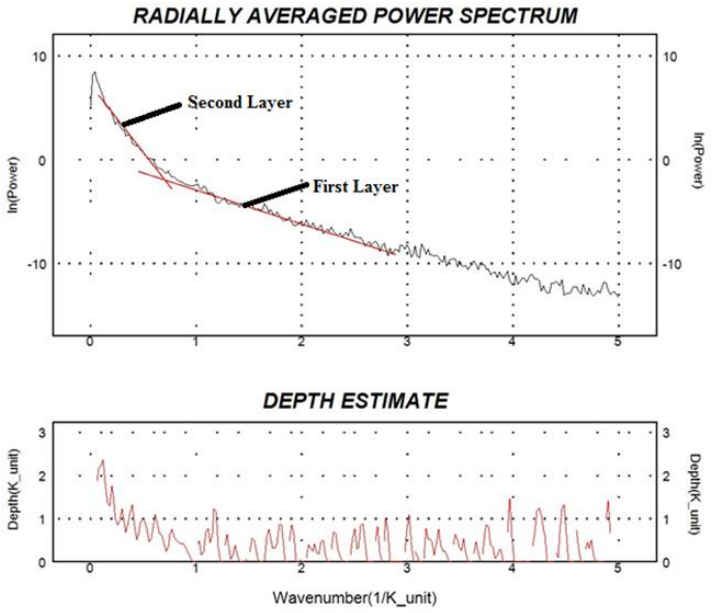

Figure 10. Spectral plot for Window 16

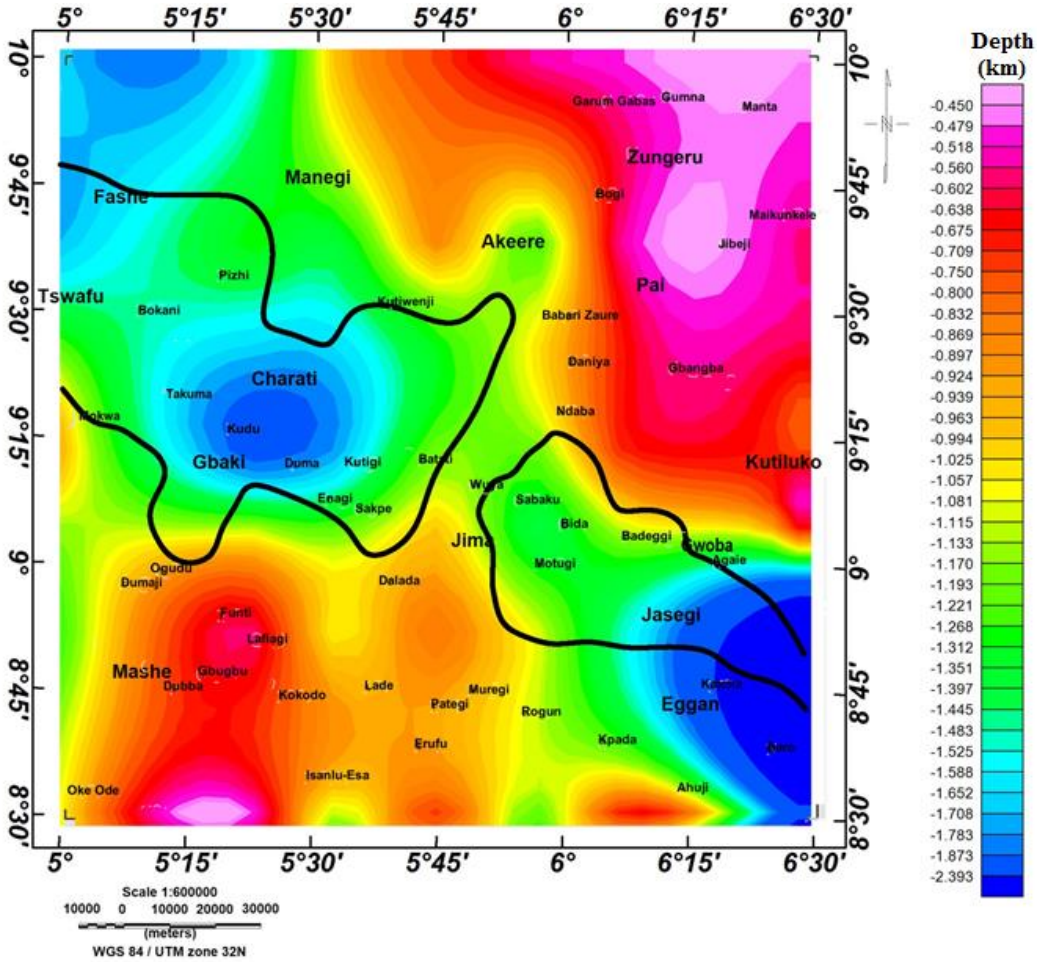

Figure 11. Depth to basement map of the study area from spectral analysis

Table 1. Slope and depth estimates of magnetic layers of the study area

S/N	X (m) (Easting)	Y (m) (Northing)	Slope of Second Layer	Slope of First Layer	Depth of L2 (km)	Depth of L1 (km)
1	64000	943900	-12.44	-4.30	0.99	0.34
2	100625	943900	-6.16	-3.49	0.49	0.28
3	121487.5	943900	-13.95	-3.20	1.11	0.25
4	142350	943900	-9.17	-4.72	0.73	0.38
5	163212.5	943900	-15.08	-4.96	1.2	0.39
6	184075	943900	-8.80	-4.21	0.7	0.33
7	221000	943900	-27.78	-6.14	2.21	0.49
8	221000	982050	-42.86	-9.12	3.41	0.73
9	184075	982050	-19.23	-4.01	1.53	0.32
10	163212.5	982050	-13.45	-4.49	1.07	0.36
11	142350	982050	-10.43	-8.23	0.83	0.65
12	121487.5	982050	-13.70	-4.31	1.09	0.34
13	100625	982050	-7.04	-3.16	0.56	0.25
14	64000	982050	-14.96	-4.46	1.19	0.36
15	64000	1003125	-14.33	-4.71	1.14	0.37
16	100625	1003125	-12.95	-3.33	1.03	0.26
17	121487.5	1003125	-14.58	-4.97	1.16	0.40
18	142350	1003125	-12.19	-2.91	0.97	0.23
19	163212.5	1003125	-18.10	-6.82	1.44	0.54
20	184075	1003125	-14.20	-3.22	1.13	0.26
21	221000	1003125	-8.29	-3.58	0.66	0.29
22	221000	1024200	-9.43	-4.73	0.75	0.38
23	184075	1024200	-7.67	-3.15	0.61	0.25
24	163212.5	1024200	-15.08	-4.11	1.2	0.33
25	142350	1024200	-14.96	-3.62	1.19	0.29
26	121487.5	1024200	-22.50	-3.62	1.79	0.29
27	100625	1024200	-25.89	-3.18	2.06	0.25
28	64000	1024200	-12.95	-4.88	1.03	0.39
29	64000	1045275	-15.96	-3.23	1.27	0.26
30	100625	1045275	-20.49	-3.97	1.63	0.32
31	121487.5	1045275	-20.36	-2.94	1.62	0.23
32	142350	1045275	-16.34	-3.34	1.3	0.27
33	163212.5	1045275	-13.20	-4.51	1.05	0.36
34	184075	1045275	-8.29	-3.48	0.66	0.28
35	221000	1045275	-7.67	-4.15	0.61	0.33
36	221000	1066350	-7.16	-3.59	0.57	0.29
37	184075	1066350	-6.16	-3.18	0.49	0.25
38	163212.5	1066350	-16.09	-4.59	1.28	0.37
39	142350	1066350	-11.06	-3.84	0.88	0.31
40	121487.5	1066350	-17.60	-3.22	1.4	0.26
41	100625	1066350	-15.96	-3.61	1.27	0.29
42	64000	1066350	-20.99	-2.96	1.67	0.24
43	64000	1104800	-21.49	-7.42	1.71	0.59
44	100625	1104800	-20.49	-5.96	1.63	0.47
45	121487.5	1104800	-11.56	-4.22	0.92	0.34
46	142350	1104800	-9.55	-3.63	0.76	0.29
47	163212.5	1104800	-7.29	-4.17	0.58	0.33
48	184075	1104800	-6.28	-4.13	0.5	0.33
49	221000	1104800	-5.66	-3.40	0.45	0.27
Average depth					1.13	0.34

From the maps of SPI and SA, the areas with shallow depth to basement are noticeable in the northeastern, eastern, southwestern and southern edge of the study area. These areas are made up of the basement complex regions partly overlain by the Bida Sandstone. The sedimentary thickness increases from the southwestern and northeastern edges to the central portion of the study area. Gbaki, Kudu, Takuma, Charati and Jasegi environments appear to have the highest sedimentary thickness. Based on the average geothermal gradient of the study area ($29℃/km$) and the highest depth estimates from both SPI and SA methods, the study area may accommodate more oil than gas.

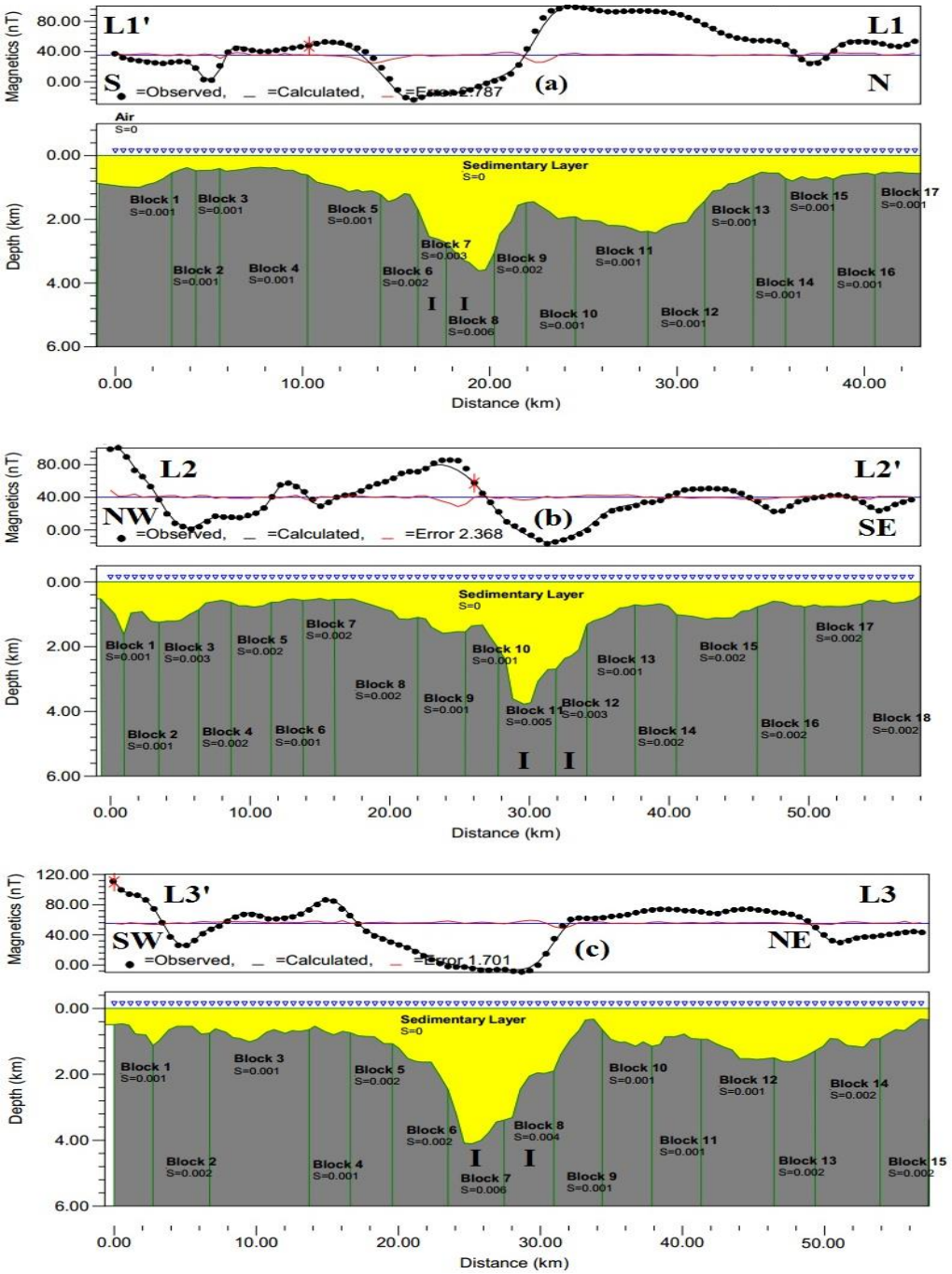

Figure 12. Magnetic profiles taken over a hydrocarbon potential area in Takuma. **I** denote Intrusive

4.5. Magnetic modelling

For an in-view of the nature of the subsurface and to delineate intrusives in potential areas of hydrocarbon generation, 2D forward modelling was carried out. This shows the compatibility of the proposed geologic model with the observed potential field data. The results from SPI technique was used as a depth constraint to estimate the sedimentary thicknesses across each profile. Magnetic profiles were drawn across the aforementioned potential areas in the N-S, NE-SW and NW-SE directions (Figure 3) to delineate intrusives around them except for Motugi and Jasegi where the profiles were taken in the N – S direction due to the uniform nature of the anomalies around these areas.

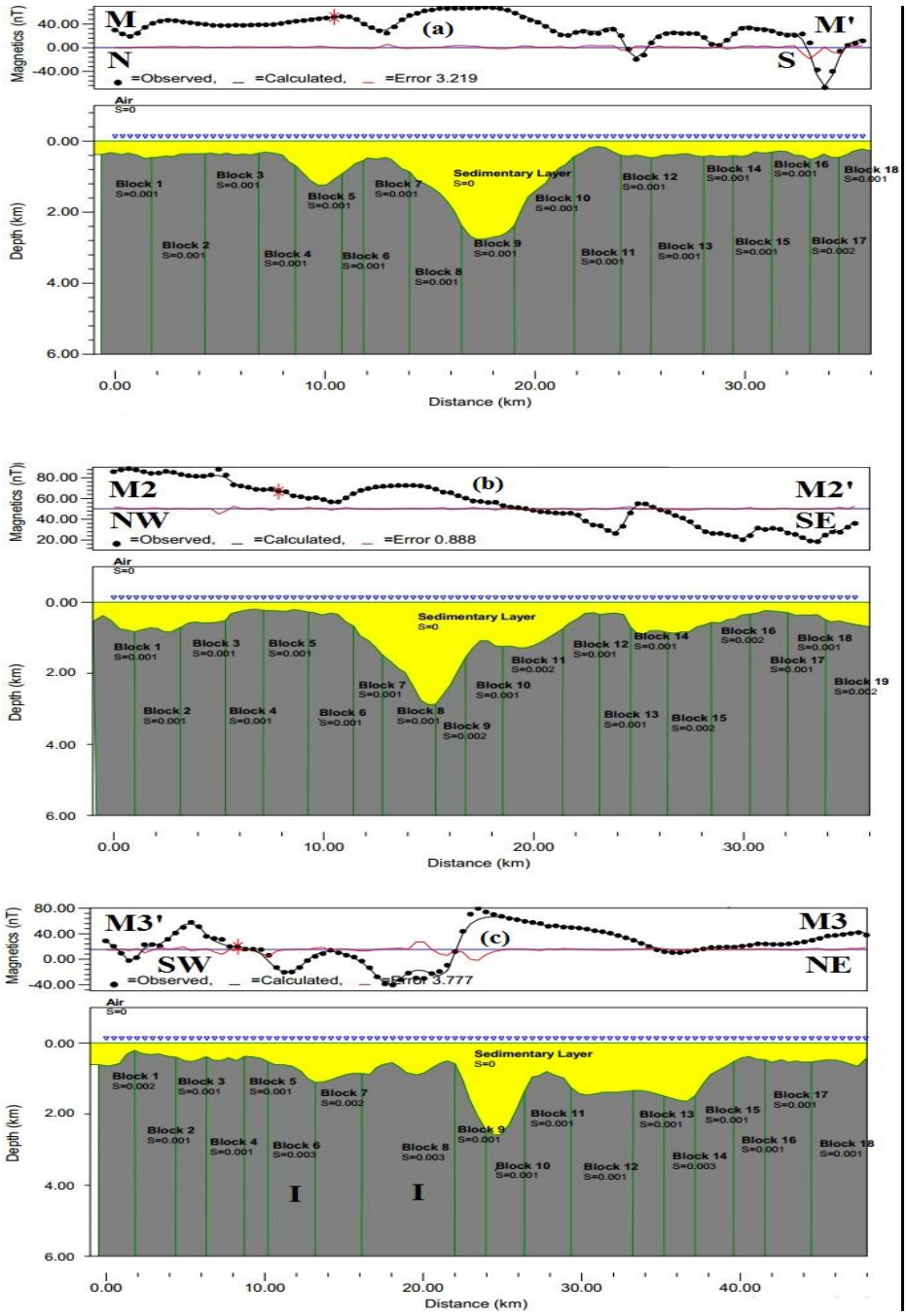

Figure 13. Magnetic profiles taken over a hydrocarbon potential area in Gbaki. **I** denote intrusive

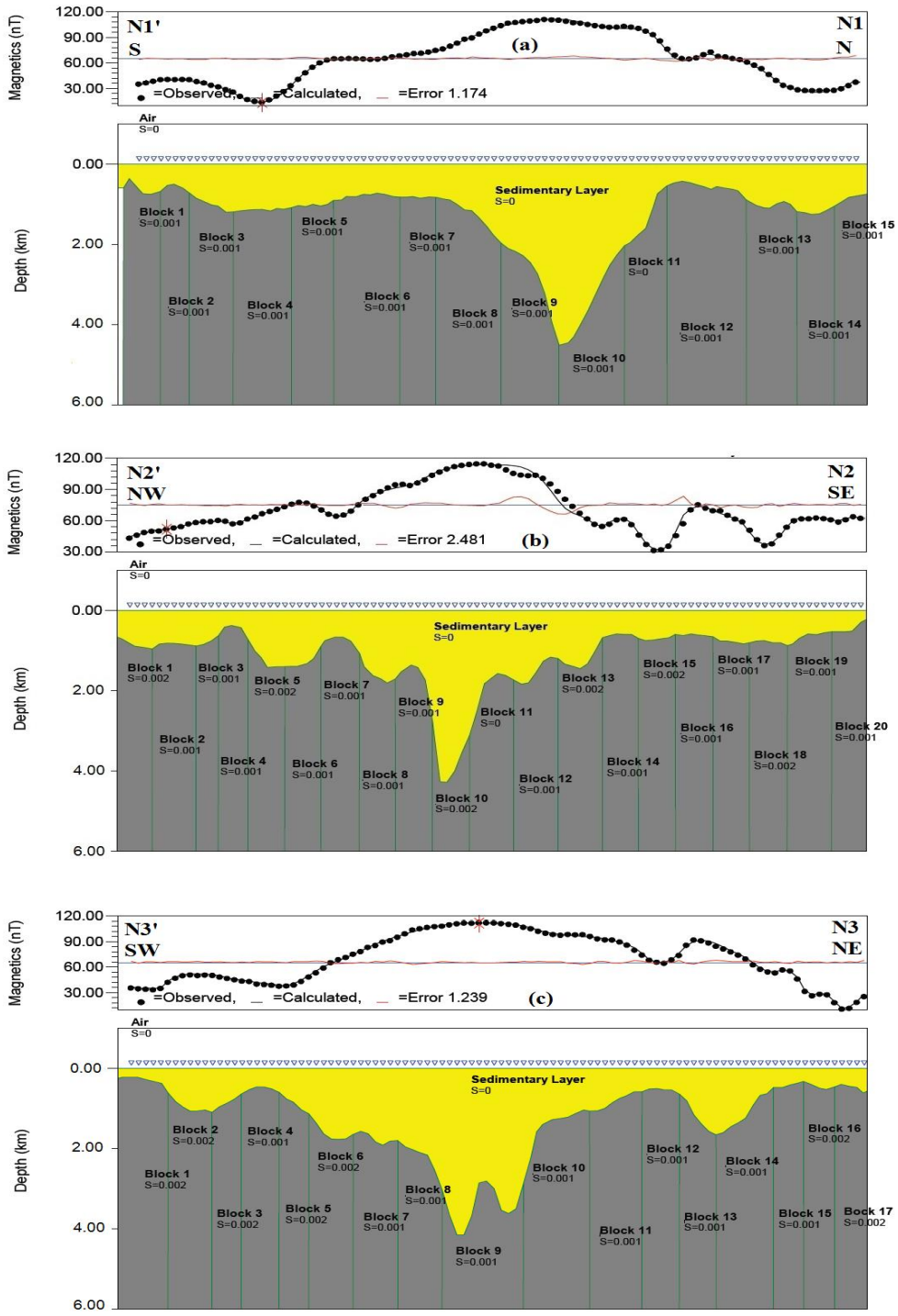

Figure 14. Magnetic profiles taken over a hydrocarbon potential area in Charati

Across all profiles, four major intrusives were inferred with lateral extent above 2 km. These intrusives have implications for hydrocarbon formation through organic matter. Across profile L1 – L1′ (Figure 12a), two major intrusives, with a susceptibility range of 0.003 – 0.006 c.g.s. at a depth of about 2 - 3.5 km, were mapped around West of Kudu (South of Takuma). These intrusives were also mapped across diagonal profiles L2 – L2′ (Figure 12b) and L3 – L3′ (Figure 12c). The intrusives fall within the oil depth window. Its implication is that source rocks within

this location will get matured faster than those close to the earths' surface. These intrusives serve as possible heat flow channels for the maturation of the Kudu Shale envisaged to be the potential source rock for hydrocarbon within the Bida Basin [5].

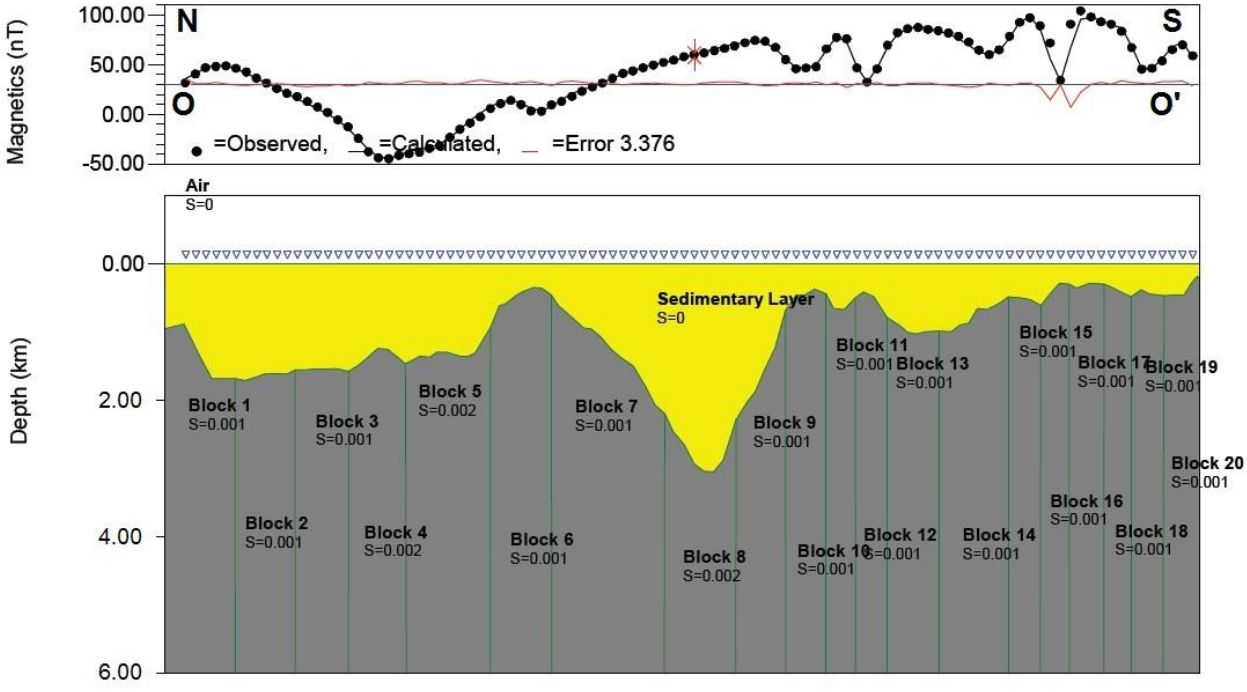

Figure 15. Magnetic profiles taken over a hydrocarbon potential area in Motugi

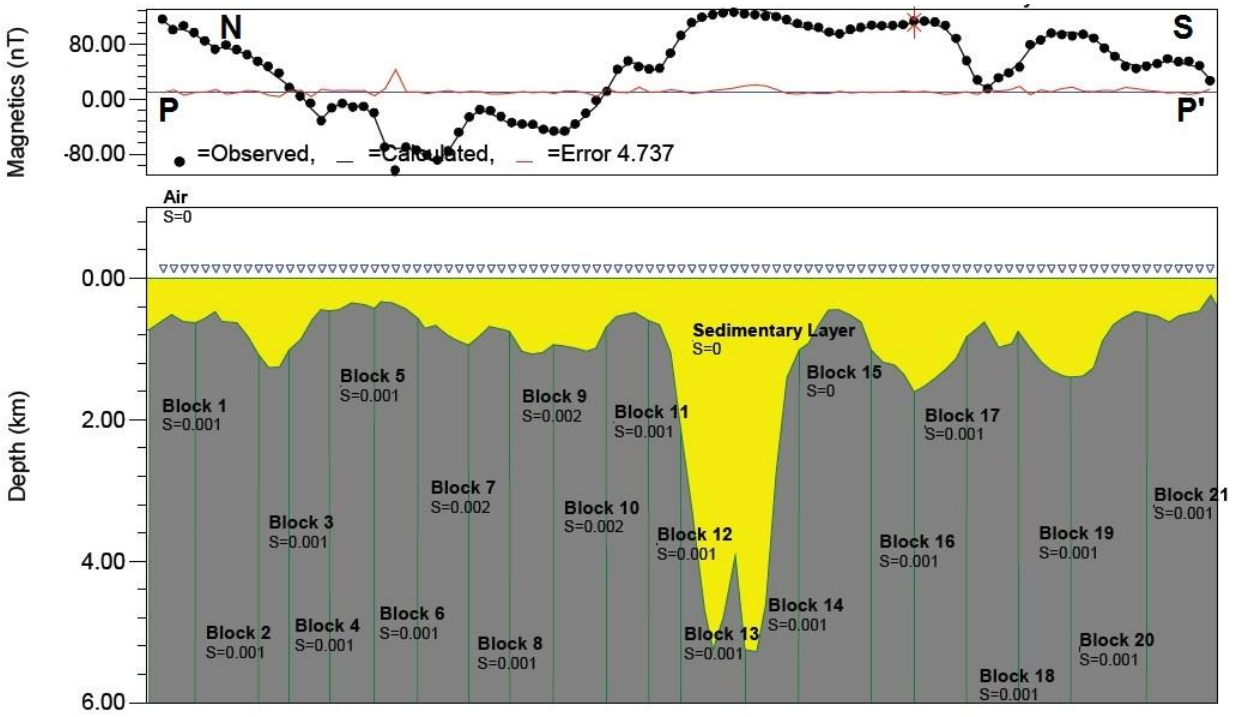

Figure 16. Magnetic profiles taken over a hydrocarbon potential area in Jasegi

Within Gbaki, two intrusives with a susceptibility of 0.003 were mapped at the western part of the study area (Profile M3' – M3, Figure 13c) occurring at depths of about 1 km. Based on

the average geothermal gradient computed for the study area, the temperature at this depth may not be enough for source rock maturation. Across Charati (Profiles N1′ – N1, N2′ – N2 and N3′ – N3), Motugi (Profile O-O′) and Jasegi (Profile P-P′), Figures 14, 15 and 16 respectively, no intrusives were mapped. Based on the results from modeling and the estimated hydrocarbon generation depth windows for the study area, Kudu and Takuma are more promising for hydrocarbon generation than other potential locations. Generally, the few number of intrusives mapped within these potential locations suggest a slow heat rate generation mechanism which implies that the source rocks within the study area could take long to mature.

5. Conclusion

The geothermal gradient and sedimentary thicknesses estimated for the study area revealed that Takuma, Kudu, Gbaki, Charati, Motugi and Jasegi areas are potential areas for hydrocarbon generation in Bida Basin. Based on the sedimentary thicknesses, average geothermal gradient and intrusives delineated within potential areas for hydrocarbon generation, this study concluded that the study area may contain more oil than gas and that Kudu and Takuma regions are more promising for hydrocarbon generation than other potential locations.

References

[1] Ali I, Olatunji S, Nwankwo SI, Akoshile CO, Johnson LM and Edino F. Geomagnetic modeling of potential hydrocarbon traps in the lower Niger Delta, Offshore West Africa. Archives of Applied Science Research, 2012; 4(2): 863-874.

[2] Selley RC. Elements of petroleum geology. 2nd Edition; Academic Press: NewYork, 1998; p. 90-97

[3] Obi DA, Okereke CS, Obei BC, and George AM. Aeromagnetic modeling of subsurface intrusives and its implication on hydrocarbon evaluation of the Lower Benue Trough, Nigeria. European Journal of Scientific Research, 2010; 47: 347-361.

[4] Rateau R, Schofield N and Smith M. The potential role of igneous intrusions on hydrocarbon migration, west of Shetland. Petroleum Geoscience. 2013; 19: 259–272.

[5] Obaje NG, Balogun DO, Idris-Nda A, Goro IA, Ibrahim SI, Musa MK., Dantata SH, Yusuf I, Mamud-Dadi and Kolo IA. Preliminary integrated hydrocarbon prospectivity evaluation of the Bida Basin in Northcentral Nigeria. Petroleum Technology Development Journal. 2013; 3(2): 36-65.

[6] Adeleye DR. Origin of ironstones: an example from Middle Niger Valley, Nigeria. Journal Sedimentary Petrol. 1973. In: Nwankwo L.I. et al., Heat Flow Anomalies from the Spectral analysis of Airborne Magnetic Data of Nupe Basin, Nigeria. 2011; 43: 709-727.

[7] Obaje NG. Geology and mineral resources of Nigeria; Springer Dordrecht Heidelberg: London New York; 2009; p. 95.

[8] Blakely RJ. Potential theory in gravity and magnetic applications. Cambridge University Press: Cambridge; 1996; p. 333.

[9] Jayeoba, A and Odumade, D. Geological and structural interpretation of Ado-Ekiti Southwest and its adjoining areas using aeromagnetic data. Pacific Section AAPG, SEG and SEPM Joint Technical Conference expanded abstracts, Oxnard, California, 2015.

[10] Geosoft, Magmap filtering how to guide: defining and applying filters and inverse fft in MAGMAP, 2015. p. 23.

[11] Okubo Y, Graf RJ, Hansent RO, Ogawa K and Tsu H. Curie point depths of the island of Kyushu and surrounding areas Japan, Geophysics. 1985; 53: 481–494.

[12] Bhattacharyya BK. and Leu LK., Analysis of magnetic anomalies over Yellowstone National Park: mapping of Curie point isothermal surface for geothermal reconnaissance, J Geophys Res. 1975; 80: 4461–4465.

[13] Spector A and Grant F. Statistical models for interpreting aeromagnetic data, Geophysics. 1970; 35: 293–302.

[14] Stampolidis A, Kane I, Tsokas GN and Tsourlos P. Curie point depths of Albania from ground total field magnetic data, Survey Geophysics. 2005; 26: 461–480.

[15] Nwankwo LI and Shehu AT. Evaluation of Curie-point depths, geothermal gradients and near-surface heat flow from high-resolution aeromagnetic (HRAM) data of the entire Sokoto Basin, Nigeria. J Volcanol Geotherm Res. 2015; 305: 45–55.
[16] Thurston JB and Smith RS. Automatic conversion of magnetic data to depth, dip, and susceptibility contrast using the SPI method, Geophysics. 1997; 62(3): 807–813.
[17] Nabighian MN. The analytic signal of two-dimensional magnetic bodies with polygonal cross-section: its properties and use for automated anomaly interpretation, Geophysics. 1972; 37(3): 507–517.
[18] Nwankwo LI, Olasehinde PI and Akoshile CO. Spectral analysis of aeromagnetic anomalies of the Northern Nupe Basin, West Central Nigeria, Global Journal of Pure and applied Sciences. 2008: 14(2): 247 – 252.
[19] Bemsen I.E, Godwin OA, Kenechukwu AE, Ifeanyi CA, Ojonugwa UA and Chukwunonso OC. Spectral analysis of aeromagnetic data over part of the Southern Bida Basin, West-Central Nigeria. International Journal of Fundamental Physical Sciences. 2013: 3(2): 27-31.

To whom correspondence should be addressed: M. O. Awoyemi, Department of Physics and Engineering Physics, Obafemi Awolowo University, Ile-Ife, Nigeria